Journal of Computational Electronics 3: 117–133, 2004
© 2004 Kluwer Academic Publishers. *Manufactured in The Netherlands.*

A Poisson P^{3}M Force Field Scheme for Particle-Based Simulations of Ionic Liquids

S. ABOUD
Molecular Biophysics Department, Rush University, Chicago, IL, USA

D. MARREIRO AND M. SARANITI*
Electrical and Computer Engineering Department, Illinois Institute of Technology, Chicago, IL, USA
saraniti@iit.edu

R. EISENBERG
Molecular Biophysics Department, Rush University, Chicago, IL, USA

Abstract. In this work we propose a force-field scheme for the self-consistent particle-based simulation of electrolytic solutions. Within this approach, the electrostatic interactions are modeled with a particle-particle-particle-mesh (P^{3}M) algorithm, where the long-range components of the force are resolved in real space with an iterative multi-grid Poisson solver. Simulations are performed where the solute ions are treated as Brownian particles governed by the full Langevin equation, while the effects of the solvent are accounted for with the implicit solvent model. The main motivation of this work is to efficiently extend the modeling capability of the standard particle-based approaches to liquid systems characterized by a spatially inhomogeneous charge distribution and realistic, non-periodic boundary conditions. Examples of such systems are large polymer chains, biological membranes, and ion channels.

Keywords: ionic solutions, Brownian dynamics, molecular dynamics, force field, ion channels

1. Introduction

The work presented in this document was motivated by the need of an improved force field scheme for the particle-based simulation of ion channel systems. Ion channels are proteins embedded in the lipid membrane of biological cells, they interact in a complex way with their environment and are responsible for finely regulating the flux of ionic charge across the membrane. For instance, the generation and transmission of potentials in nerves and muscles, as well as the hormone release from endocrine cells, are believed to be mechanisms governed by the transport of ionic charge through these protein "gates" [1].

Since the first demonstration in 1976 [2] of a reliable experimental methodology for the detection of currents flowing through individual ion channels, several refinements of the experimental setup have been successfully applied to a variety of membrane and cell configurations, both *in vivo* and *in vitro*. The extraordinary progress of the experimental techniques triggered an increasing theoretical effort aimed at the understanding of the role of ion channels in the physiology of complex biological systems, and, more generally, their influence on the electrical equilibrium between the cells and their environment. Besides the purely theoretical aspect, the enormous pharmacological advances expected from the knowledge of the operation mechanisms in ion channels has been one of the strongest arguments in favor of their research [3]. Furthermore,

*To whom correspondence should be addressed.

from an engineering viewpoint, ion channels are being envisioned as a key component of a new generation of bio-sensors that integrate the selectivity and the extreme sensitivity of ion channels with the processing capabilities of modern microelectronics [4].

A quite peculiar aspect of the research on ion channels is that it frequently involves researchers working in traditionally different disciplines. The solid-state electronics community, for example, is well aware of the fact that traditional scaling—i.e. the reduction of the feature-size of transistors in order to increase the performance of integrated circuits [5]—will soon be inadequate to satisfy the requirements of emerging technologies [6]. A natural solution is to increase the complexity rather than the speed of the basic components, and much can be learned from ion channels, which are extremely specialized and miniaturized low power devices. Transistors are definitely faster than ion channels, but the advantage due to their operational speed is compensated by the complexity of the operations performed by ion channels. The full understanding of ion channels properties will allow for either the modification of their design for novel applications, or for manufacturing analogous structures capable of emulating their functionality. It is safe to say that the capability of explaining the functions of ion channels in relation to their microscopic structure would make possible the realization of man-made devices, such as nanotubes, that are based on the same principles that regulate their natural counterparts, and perform operations with the same level of complexity.

A hierarchy of simulative approaches has been applied to the study of ion channels during the last two decades. Continuum models, such as the Poisson-Boltzmann [7] and the Poisson-Nernst-Plank [8], have been used to define the electrostatic landscape of ion-channel systems and to analyze ion electrodiffusion in terms of continuous fluxes. Individual ionic trajectories have been studied using particle-based approaches subjected to both Brownian [9] and Newtonian dynamics [10]. This document focuses on the approach used to compute the self-consistent field of forces used by particle-based simulation algorithms. In this context, the adjective *self-consistent* refers to the fact that the forces due to the electrostatic interactions within the components of the system strictly depend on the spatial configuration of the components themselves, and must be continuously updated as the dynamics of the system evolves.

The most straightforward approach to compute the force on a given charged particle is based on Coulomb's law, and consists of directly summing the pairwise contributions from all the other particles in the system. The performance of this Particle-Particle (PP) approach scales quadratically with the particle population, making its implementation impractical for the simulation of large systems. Based on a screening hypothesis [11], a finite cut-off radius can be used to improve the overall performance of the PP method by reducing the number of particles involved in the calculation. This technique neglects long-range coulombic forces that can be determinant [12,13], particularly when the charge is inhomogeneously distributed within the computational domain, or when the effects of the force field are investigated on large molecular structures. Furthermore, accounting for inhomogeneous dielectric boundaries and external bias is extremely difficult within the framework of Coulomb's equation. Indeed, a complicated dynamic distribution of image charges [14] needs to be added to the system in order to represent the effects of realistic boundary conditions.

Alternatively, Particle-Mesh (PM) methods [15] are used to compute the electrostatic forces due to the charge distribution of the whole system, and naturally allow for the inclusion of boundary conditions by setting the potential or its derivative on the surfaces of the computational domain. Within the PM framework, the charge distribution is mapped onto a discrete set of points (the mesh or grid points), and the corresponding electrostatic potential is computed on the same points with a standard numerical technique. Forces are then interpolated from the grid to the arbitrary positions of the charged particles in the system. An evident advantage of the PM approach is that it scales linearly with the number of charged particles and, in some cases [16], with the number of grid points.

The PM method has been successfully used for the simulation of semiconductor devices [15], and has the advantage of efficiently modeling systems with dielectric interfaces, highly complex geometries, and arbitrary boundary conditions. However, within the PM approach the resolution of the charge distribution is limited to the mesh size, therefore short-range effects are not accounted for in the force field. This does not constitute a problem for the simulation of electron devices in the framework of the independent electron approximation [17], or when short-range coulombic interactions are treated statistically with perturbation theory [18]. It is worthwhile to note that works have

been published recently [19,20] where the short-range interaction between charge carriers in semiconductor devices is computed with the PP method and coupled with the PM approach.

Neglecting the short-range structure of the force field is unrealistic in the case of molecular liquid systems because of the finite size of the various components. In other words, the exponential van der Waals forces arising from the overlapping electronic orbitals of adjacent molecules (or atoms) [21] play a crucial role in the microscopic dynamics of ionic solutions. This is also true for charge transport across ion channels, which use atomic scale interactions to control the macroscopic flow of ions driven by long-range forces. For this reason, a realistic force field scheme must have a spatial resolution adequate to model the van der Waals interaction, and therefore couple effectively and accurately both the short- and long-range electrostatics of the system [15].

Two mathematically similar [22] methods that combine the PM and PP approaches in an unified field solver are the the Ewald summation method [23] and the particle-particle-particle-mesh (P^{3}M) approach [15]. In spite of their theoretical affinity, the implementation of the two approaches shows substantial differences that motivate our preference of the latter for the simulation of inhomogeneous ionic solutions. Within both models, the electrostatic force field is separated into two smoothly varying functions representing the short-range and long-range forces. The PP approach is used to model the short-range component within a relatively small cutoff region, while different methods are used to compute the long-range interactions. In particular, the Ewald method computes the short-range forces in real space, while long-range interactions are rapidly accounted for in the reciprocal space. A crucial effect of this approach is the rather stringent requirement of spatial periodicity for the charge distribution function [24]. This fact does not constitute a problem in the simulation of bulk systems, provided that the periodicity does not introduce artifacts (e.g., spurious numerical heating of the system), and sufficient spatial resolution is maintained to describe large scale order relevant for atomic scale behavior, but limits its applicability in systems with complex boundaries. On the other hand, within the P^{3}M method, the long-range interactions are computed in real space with a PM approach [15], making it the optimal choice for modeling inhomogeneous systems with external bias values. In both the Ewald and the P^{3}M method a geometric overlap exists between the long-range and short-range computational domains, i.e. the short-range domain is fully contained by the long-range one. Consequently, both schemes include a correction that accounts for the fact that charges within the short-range domain are also used for the long-range calculation.

The approach we propose in this work extends and validates the original P^{3}M method of Hockney [15] by including a highly efficient real-space 3D Poisson solver based on the iterative multi-grid method [16,25]. The use of a Poisson solver in determining the long range electrostatic forces for a molecular liquid system is not a new approach, but its use has been limited in the past due a claim that obtaining its numerical solution is computationally prohibitive [26–28]. We assert that the numerical solution of the Poisson equation can be implemented in a computationally efficient manner for systems of arbitrary geometry and boundary conditions.

To validate the proposed force field scheme, the Poisson-based P^{3}M algorithm is coupled with a Brownian dynamics (BD) [29,30] kernel. The BD approach is an efficient particle-based method for simulating large ionic liquid systems for relatively long times. The BD method has been applied to a wide range of many-body problems, such as the simulation of bulk ionic solutions [29–31], the permeation of ions through membrane channels [9,28,32–37], and the steady-state properties of electron transport in semiconductor devices [38]. Within the BD framework, the trajectories of the individual ions are tracked through phase-space, while the surrounding solvent medium is modeled as a continuum dielectric according to the implicit solvent model. The ions and the solvent are then coupled through electrostatic, hydrodynamic and stochastic forces. Observable properties of the system are calculated by averaging over a sufficiently large number of ion trajectories. The computational burden is greatly reduced by including the effects of solvent molecules implicitly, so allowing for long simulation times. This fact motivated our choice of a BD kernel for the validation of the proposed force-field scheme. However, the proposed approach is fully applicable to molecular dynamics (MD) [39] simulations. It is worthwhile to note that many variants of the BD simulation kernel are possible, including the ones based on the Smoluchowski equations of motion [40] and the Langevin equation [11]. Memory effects can be included in the model [41], as well as hydrodynamic interactions [42–44].

This paper is organized as follows. In the proceeding section the dynamics simulation kernel used to validate the force-field scheme is briefly presented. The approach used to resolve the electrostatic interaction is then discussed in the following section. Details about the implementation of the proposed force-field scheme will be supplied. Finally, the results of the simulation of different electrolytic solutions are discussed, and comparisons with other models and with experimental data are offered.

2. Brownian Dynamics

Within the chosen BD framework, the solvent (water) is treated as a continuum dielectric, while each ion is explicitly modeled as a Brownian particle with its dynamics being tracked through the 6-dimensional phase space. The field distribution is periodically updated on the 3D computational domain, where the ion-solvent interactions are accounted for by including macroscopic water properties in the model. In other words, the dynamics of the ions is *explicitly* determined by the electrostatics of the system through Newtonian mechanics, while their interaction with water molecules is *implicitly* modeled with the Langevin equation. The observable properties of the system are then extracted from the microscopic representation of the ions by averaging over the ionic ensemble and over time after the steady state is reached [45]. It should be noted that the further inclusion of complex molecules such as lipid conglomerates or proteins can be achieved both in a macroscopic fashion by adding dielectric discontinuities to the computational domain, and microscopically, by building collections of van der Waals particles subjected to an appropriate constrained dynamics. The latter approach allows for the study of effects related to the time evolution of the structural properties of the molecules in the system.

The next sections will be devoted to the brief discussion of the dynamics equations used by the implemented BD kernel and the methodology used to integrate them.

2.1. Langevin Equation

The dynamics simulation engine used to validate the proposed force field scheme models ion trajectories within the Langevin formalism [29,30]. In particular, the strict or full Langevin equation is used, which assumes Markovian random forces and neglects correlations (both spatially and temporally) of the ionic motion:

$$m_i \frac{d\vec{v}_i(t)}{dt} = -m_i \gamma \vec{v}_i(t) + \vec{F}_i(\vec{r}_i(t)) + \vec{B}_i(t), \quad (1)$$

where m_i is the reduced mass of the ith ion, $\vec{v}_i(t)$ is its velocity at time t, and γ is the friction coefficient (i.e., the inverse of the velocity relaxation time). The definition of the friction coefficient in the Langevin equation varies in literature [11,45,46], the notation used here is the same as in the work of Gunsteren and Berendsen [46]. The force on particle i due to all other particles in the system and boundary conditions (including internal dielectric discontinuities) is $\vec{F}_i$, while $\vec{B}_i$ is a fluctuating force that mimics the molecular bombardment of water on the ions, and is modeled with a Markovian random variable.

The Langevin equation is discretized temporally by a set of equally spaced time intervals, and spatially onto a tensor-product Cartesian grid. At predetermined times the ion dynamics is frozen, and the spatial distribution of the force is calculated from the vector sum of all its components, including both the long- and short-range contributions. The components of the force are then kept constant while the dynamics resumes under the effect of the updated field distribution. Self-consistency between the force field and the ionic motion in the phase-space is obtained by iterating this procedure for a desired amount of simulation time. The choice of the spatial and temporal discretization schemes plays a crucial role in terms of computational performance and model accuracy.

The integration scheme for Eq. (1) is chosen based on two requirements: ensuring energy stability and allowing for long time-steps [47]. The latter requirement is related to the need for investigating the properties of the system over the typically long biological and/or chemical time scales, which can extend up to milliseconds. The use of long time-steps reduces the number of operations for each unit of simulated time, consequently increasing the performance of the simulation code. On the other hand, the time-step must be small compared with the mean time between particle collisions. An excessively coarse time discretization would not account for rapid variations of the short-range force, and fails to correctly account for the coulombic singularity. This typically results in a spurious heating of the particle ensemble that becomes energetically unstable [15,48].

Two integration schemes have been implemented: the standard first-order Euler scheme and the *Verlet-like* method by Gunsteren and Berendsen [46], which is a third order model that reduces to the Verlet algorithm [49] when the friction coefficient in the Langevin equation is zero. This approach allows for a larger time-step as compared to the Euler method. Both schemes are discussed in the following sections, and comparisons are made.

2.2. Euler Integration

The first order Euler integration scheme reduces the Langevin equation to the following expression:

$$\vec{v}_i(t+\Delta t) = \vec{v}_i(t) - \Delta t\left[\gamma\vec{v}_i(t) - \frac{\vec{F}_i}{m_i} - \sqrt{\frac{2\gamma k_B T}{m_i \Delta t}}\vec{N}(0,1)\right], \tag{2}$$

where Δt is the integration time-step and $\vec{N}(0,1)$ is a three dimensional Gaussian random variable with zero mean and variance 1. The spatial trajectories are calculated with Newtonian mechanics. A crucial aspect of the Euler scheme is that in order to represent the fluctuating force as a stationary Markovian Gaussian process, the time-step Δt duration must be much smaller than the reciprocal of the friction coefficient γ in the Langevin equation (Eq. (1)) [46]. This results in a fine (and computationally expensive) time discretization when ionic solutions are simulated.

2.3. Verlet-Like Integration

The short time-steps limitation of the Euler integration scheme is addressed within the Gunsteren and Berendsen approach [46] by accounting for the evolution of the fluctuating force during the integration time-step. In this method, the force on the ith particle at time t_{n+1} is first expanded in a power series about the previous time t_n:

$$F_i(t_{n+1}) \sim F_i(t_n) + \dot{F}_i(t_n)(t_{n+1} - t_n), \tag{3}$$

where $\dot{F}$ denotes the time derivative. The power series expansion is substituted into Eq. (1), and the resulting solution of the Langevin equation is given by

$$\begin{aligned} v_i(t_{n+1}) = {} & v_i(t_n)e^{-\gamma\Delta t} + (m_i\gamma)^{-1}F_i(t_n)(1-e^{-\gamma\Delta t}) \\ & + (m_i\gamma^2)^{-1}\dot{F}_i(t_n)(\gamma\Delta t - (1-e^{-\gamma\Delta t})) \\ & + (m_i)^{-1}e^{-\gamma\Delta t}\int_{t_n}^{t} e^{-\gamma(t'-t_n)}B_i(t')dt', \end{aligned} \tag{4}$$

where $\Delta t = t_{n+1} - t_n$ is the integration time-step. Note that the fluctuating force $B_i(t)$ is left inside the integral. The ionic position is calculated with the following expression:

$$\begin{aligned} x_i(t_{n+1}) = {} & 2x_i(t_n) - x_i(t_{n-1})e^{-\gamma\Delta t} \\ & + \int_{t_n}^{t_n+\Delta t} v_i(t')dt' + e^{-\gamma\Delta t}\int_{t_n-\Delta t}^{t_n} v_i(t')dt', \end{aligned} \tag{5}$$

and, finally, the updated particle position is written as

$$\begin{aligned} x_i(t_{n+1}) = {} & x_i(t_n)[1+e^{-\gamma\Delta t}] - x_i(t_{n-1})e^{-\gamma\Delta t} \\ & + (m_i\gamma)^{-1}F_i(t_n)(\Delta t)[1-e^{-\gamma\Delta t}] \\ & + (m_i\gamma^2)^{-1}\dot{F}_i(t_n)(\Delta t)[0.5\gamma\Delta t(1+e^{-\gamma\Delta t})] \\ & - [1-e^{-\gamma\Delta t}] + X_i^n(0,\Delta t) \\ & + e^{-\gamma\Delta t}]X_i^n(0,-\Delta t). \end{aligned} \tag{6}$$

where

$$\begin{aligned} X_i^n(0,\Delta t) = {} & (m_i\gamma)^{-1}\int_{t_n}^{t_n+\Delta t}\left[1-e^{-\gamma(t_n+\Delta t-t')}\right] \\ & \times B_i(t')dt' \end{aligned} \tag{7}$$

is also a Markovian stochastic process with zero mean and variance Δt. The function $X_i^n(0,-\Delta t)$ is correlated with $X_i^{n-1}(0,\Delta t)$ through a bivariate Gaussian distribution. In the limit that the friction coefficient goes to zero this set of equations corresponds to the trajectories obtained with the Verlet MD algorithm [46,50].

The set of trajectories resulting from the Verlet-like integration scheme are not limited by the velocity relaxation time, and a longer time-step can be used as compared to the Euler scheme. Figure 1 shows a plot of the steady-state average ionic energy versus the time-step length for a 150 mM KCl solution simulated for 1 ns in the absence of an external electric field. The Euler and Verlet-like algorithms give similar results for time-steps below approximately 10 fs, but larger time-steps result in a high energy drift for the Euler integration.

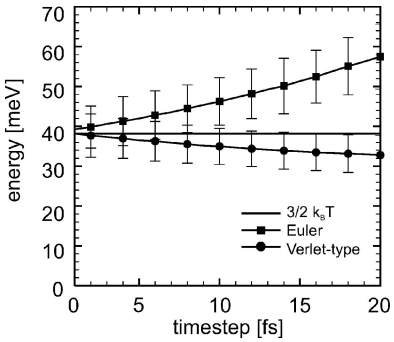

Figure 1. Steady-state energy of an ensemble of anions and cations in a 150 mM solution of KCl as a function of the time-step length, for both the Euler and Verlet-like integration schemes.

3. Poisson P^{3}M Force Field

Within the proposed approach, the force on an individual ion is divided into a smoothly varying long-range component and a short-range part. Both components are periodically updated in a fashion consistent with the ionic dynamics, as explained in Section 2.1. The long-range interaction accounts for the force due to the collective ionic population and the boundary conditions, while the short-range inter-particle interactions result from the coulombic and van der Waals forces between close ions. The total force acting on a particle i is then written as follows:

$$\vec{F}_i = \vec{F}_i^{pm} + \vec{F}_i^{pp}. \tag{8}$$

The long range particle-mesh force $\vec{F}_i^{pm}$ is obtained by assigning the charge density to the grid points, solving Poisson's equation [14], and differentiating the potential:

$$\vec{F}^{pm}(\vec{r}_p) = -q\vec{\nabla}\phi(\vec{r}_p) \tag{9}$$

where $\vec{F}^{pm}$ and $\phi(\vec{r}_p)$ are the force and the electrostatic potential, respectively, at the grid point p located at $\vec{r}_p$. This component of the force also accounts for external boundary conditions, dielectric discontinuities, and static charges. The force $\vec{F}_i^{pm}$ at the specific position $\vec{r}_i$ of the ion i is then computed by an appropriate interpolation scheme (see Section 3.1).

The particle-particle force is decomposed in three parts:

$$\vec{F}_i^{pp} = \vec{F}_i^{C} + \vec{F}_i^{W} + \vec{R}_i, \tag{10}$$

where $\vec{F}_i^{C}$ is the coulombic force due to all the particles within a predefined short-range domain (see Section 3.2), $\vec{F}_i^{W}$ represents the effects of the van der Waals forces, and, finally, $\vec{R}_i$ is a "reference force" [15] that corrects the double counting of charges due to the overlap between the short-range domain and the entire computational region over which Poisson's equation is solved.

A detailed description of all the components of the force $\vec{F}_i(\vec{r}_i)$ is given in the following sections.

3.1. Long Range Interaction, Poisson's Equation

In order to solve Poisson's equation on a mesh, a charge assignment scheme must be devised to build a charge distribution from the ionic coordinates. Furthermore, once the electrostatic field has been computed on the grid from the solution of Poisson's equation, the force must be interpolated to each ion location in a way that is consistent with the original charge assignment scheme. In other words, a geometric shape is assigned to each ion charge though a space-dependent weighting function $W(\vec{r})$ [15], and the relation between the charge shape and the discretization grid is accounted for in all the transformations used to transfer quantities (i.e. charge and force) to and from the discrete mesh centered at $\vec{r}_p$.

The generalized algorithm follows the treatment of Hockney [15]:

1. *Assign charge*:

$$\rho(\vec{r}_p) = \frac{1}{V_p}\sum_{i}^{N_p} q_i W(\vec{r}_i - \vec{r}_p); \tag{11}$$

2. *Solve Poisson's equation*:

$$\vec{\nabla}\cdot\epsilon_r\vec{\nabla}\phi(\vec{r}_p) = -\frac{\rho(\vec{r}_p)}{\epsilon_0}; \tag{12}$$

3. *Calculate electric field*:

$$\vec{E}(\vec{r}_p) = -\vec{\nabla}\phi(\vec{r}_p); \tag{13}$$

4. *Interpolate force*:

$$\vec{F}_i^{pm}(\vec{r}_i) = \sum_{p}^{N_p} q_i W(\vec{r}_i - \vec{r}_p)\vec{E}(\vec{r}_p); \tag{14}$$

where V_p and N_p are the volume of the grid cell and the number of particles in it, respectively, and $\vec{F}_i^{pm}$ is the long-range component of the force acting on the particle located at $\vec{r}_i$ (see Eq. (8)). It should be noted that the same function $W(\vec{r})$ must be used both for the charge assignment and for the force interpolation, because the use of a mixed scheme would result in an unphysical self-force of the particle upon itself. The choice of the weighting function depends on the properties of the system. The three models implemented and tested in this work treat the particle as a point charge, an uniformly charged sphere, and a sphere with a linearly decreasing density; the corresponding assignment schemes are called the nearest-grid point (NGP), the cloud-in-cell (CIC) and the triangular-shaped cloud (TSC) schemes, respectively [15].

Once a charge shape has been chosen, the corresponding weighting function is determined by the following integral,

$$W(\vec{r} - \vec{r}_p) = \int_{V_p} S(\vec{r'} - \vec{r})\, d\vec{r'}, \tag{15}$$

where the function $S(\vec{r})$ represents the shape of the charge "cloud" associated with the particle. In one dimension, the weighting functions computed from Eq. (15) are given by the following relations for the three charge shapes mentioned above:

$$W_{NGP}(x) = \begin{cases} 1 & \left|\frac{x}{H}\right| \le \frac{1}{2} \\ 0 & \text{otherwise} \end{cases}, \tag{16}$$

$$W_{CIC}(x) = \begin{cases} 1 - \left|\frac{x}{H}\right| & \left|\frac{x}{H}\right| \le 1 \\ 0 & \text{otherwise} \end{cases}, \tag{17}$$

$$W_{TSC}(x) = \begin{cases} \frac{3}{4} - \left|\frac{x}{H}\right|^2 & \left|\frac{x}{H}\right| \le \frac{1}{2} \\ \frac{1}{2}\left(\frac{3}{2} - \left|\frac{x}{H}\right|\right)^2 & \frac{1}{2} \le \left|\frac{x}{H}\right| \le \frac{3}{2} \\ 0 & \text{otherwise} \end{cases}, \tag{18}$$

where H is the mesh size. In three dimensions the weighting function is obtained as follows,

$$W(\vec{r}) = W(x)W(y)W(z). \tag{19}$$

In agreement with the considerations of Hockney [15], the TSC weighting function is the optimal compromise between accuracy and computational performance for the systems studied in this work.

The use of a Poisson solver for the solution of the long-range interaction results in two main advantages: (1) the possibility of imposing boundary conditions through externally applied potentials and (2) the ability to simulate systems with arbitrary ionic concentrations at the boundaries. While the simulation of bulk homogeneous systems do not exploit these capabilities and can (should) be performed with periodic boundary conditions, the use of a Poisson solver allows for a higher degree of realism in reproducing the electrostatic configuration of inhomogeneous systems.

3.1.1. Multi-Grid Poisson Solver. The need for self-consistency between the spatial charge distribution and the field of forces directly implies a frequent solution of Poisson's equation. For this reason, the implementation of an efficient and robust Poisson solver plays a crucial part in the proposed P^{3}M scheme. Indeed, for three dimensional systems the time spent for the repeated solution of Poisson's equation becomes a significant part of the total CPU time, and the efficiency of the solver becomes an issue.

Because of the frequent solution of Poisson's equation within the self-consistent scheme, iterative solvers [51,52] are the most natural option, due to the availability of the previously computed solution as the initial guess for the solver [53]. Therefore, the method of choice in this work is a finite-difference Poisson solver based on the iterative version of the multi-grid algorithm [16,25].

Within the multi-grid approach, the matrix equation resulting from the discretization of Poisson's equation [54,55] is solved simultaneously on a set of grids with varying coarseness. The hierarchy of grids allows for the simultaneous reduction of different Fourier components of the error associated with each iteration of the solver [56]. This results in a much faster convergence rate as compared to other standard iterative methods such as the successive-over-relaxation (SOR) method [15,57]. A comparison of the total CPU time spent solving Poisson's equation for one self-consistent iteration as a function of the convergence error is shown in Fig. 2 for the multi-grid method and an optimized SOR algorithm [16]. The computational domain consists of a 100 mM KCl solution represented on a $65 \times 65 \times 65$ homogeneous grid with a mesh size of 0.5 nm in all three dimensions. The slope of the error indicates the performance behavior of the solver. As can be seen, the convergence rate of the multi-grid method is much better than the SOR, particularly at

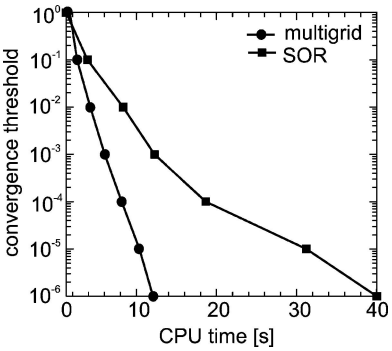

Figure 2. Comparison of the CPU time required to solve Poisson's equation by the multi-grid and SOR methods. The computational domain consists of a $65 \times 65 \times 65$ homogeneous mesh.

small values of the relative error. Convergence thresholds are typically chosen within the range $[10^{-4}$–$10^{-5}]$, and result in CPU times of 8–10 seconds for the solution using the multi-grid approach, and 20–30 seconds for the SOR.

Algorithmic details on the implementation of the multi-grid method can be found in the excellent works of Hackbusch [16] and Brandt [25,58]. It should be noted that the multi-grid approach can be easily applied to adaptive non-tensor-product grids [25,58], allowing for a variable resolution in regions of the computational domain where the charge concentration is high. Being focused on bulk properties, the simulations of this work are performed using a relatively simple tensor-product discretization grid. A discretization scheme based on adaptive grids can result in a further increase of the performance when simulating highly inhomogeneous systems such as biological membranes or complex proteins.

The choice of using the SOR solver in the P^3M proposed by Beckers [59] is not advocated here because of its slower convergence compared to the multi-grid approach, and because of its inefficiency for large problems. It is recognized, however, that the extreme simplicity of the SOR algorithm makes it an attractive choice. A typical SOR solver can be implemented with a few tens of lines of code, while our 3D multi-grid solver is several thousands lines long. Furthermore, the multi-grid choice for the Poisson solver is certainly not unique, other efficient algorithmic choices are available, such as the strongly implicit schemes [60] and the many flavors of the conjugate gradient technique [61]. Mixed schemes based either on heterogeneous preconditioning or smoothing are also possible [62]. In this work, we have chosen to use the multi-grid approach because of its efficiency, robustness, and scalability.

As a final remark, we like to briefly discuss the issue of computational performance. Clearly, the force field calculation is an important component in the budget of CPU resources used in particle-based simulation of liquids. The computational burden due to the algorithms used for long- and short-range interactions depends on the nature of the system and its size. Within the framework of ion channel simulation, one normally expects a relatively large in-homogeneous Poisson grid with at least 10^4 cells, and a larger number of particles (including the protein "fixed" charges). In this case, even though most of the burden is due to the computation of the short-range interaction, the time spent for the long-range calculation would be a significant portion of the time devoted to the full force-field algorithm. For this reason, both performance and robustness are crucial requirements when modeling the long-range interaction for ion channel systems.

3.1.2. Electric Field. The electric field used to calculate the long-range PM force is computed at each grid point as the gradient of the potential obtained from the Poisson solver. The differentiation of the potential takes into account dielectric discontinuities, possible interfacial charges and boundary conditions. The force $\vec{F}_i^{pm}$ at the specific particle location is then interpolated with the same weighting function used for charge assignment (see Eq. (14)).

3.2. Short-Range Interaction

As stated by Eq. (10), the particle-particle force is comprised of three parts: the Coulomb force $\vec{F}_i^C$, the van der Waals force $\vec{F}_i^W$, and the reference force $\vec{R}_i$:

$$\vec{F}_i^C = \sum_{j \neq i}^{\Omega_i} \frac{q_i q_j}{4\pi\epsilon_r\epsilon_0 |\vec{r}_i - \vec{r}_j|^2} \hat{r_{ij}}, \tag{20}$$

$$\vec{F}_i^W = \begin{cases} \displaystyle\sum_{j \neq i}^{\Omega_i} \frac{24\epsilon_{ij}}{|\vec{r}_i - \vec{r}_j|} \left[2\left(\frac{\sigma_{ij}}{|\vec{r}_i - \vec{r}_j|} \right)^{12} - \left(\frac{\sigma_{ij}}{|\vec{r}_i - \vec{r}_j|} \right)^{6} \right] \hat{r_{ij}} \\ \qquad\qquad \text{Lennard-Jones}, \\ \displaystyle\sum_{j \neq i}^{\Omega_i} \frac{\beta_{ij} \left| q_i q_j \right|}{4\pi\epsilon |\vec{r}_i - \vec{r}_j| (p+1)} \left(\frac{s_i + s_j}{|\vec{r}_i - \vec{r}_j|} \right)^{p} \hat{r_{ij}} \\ \qquad\qquad \text{inverse power}, \end{cases} \tag{21}$$

$$\vec{R}_i = -\sum_{j\neq i}^{\Omega_i} \frac{q_i q_j}{4\pi\epsilon_r\epsilon_0} \iint S(\vec{r}_1)S(\vec{r}_2 - \vec{r}_{ij}) \times \frac{(\vec{r}_1 - \vec{r}_2)}{|\vec{r}_1 - \vec{r}_2|^3} d\vec{r}_1 d\vec{r}_2, \quad (22)$$

where Ω_i is the domain of the short-range interaction (see below), ϵ_r is the relative dielectric constant, ϵ_0 is the permittivity of vacuum, q is the charge, and $\vec{r}_{ij}$ is the distance between the ions.

The van der Waals force $\vec{F}_i^W$ is often modeled with the Lennard-Jones function or by an inverse power relation [63]. The former has been used in this work, and is based on the two fitting parameters σ_{ij} and ϵ_{ij}, representing respectively the maximum attraction distance and the strength of the interaction [64]. For ions of different species, the Lennard-Jones parameters are calculated by combining the values of the individual species [64],

$$\sigma_{ij} = \frac{1}{2}(\sigma_i + \sigma_j), \quad \text{and,} \quad \epsilon_{ij} = \sqrt{\epsilon_i \epsilon_j}. \quad (23)$$

In the expression of the inverse power law, β_{ij} is an adjustable parameter, s_i is the radius of the ith particle, and p is a hardness parameter that also represents the strength of the interaction. A comparison of the inter-ionic potential profile is shown in Fig. 3 for the two different pair potential schemes in an aqueous KCl solution. The parameters used for the short range potentials are taken from [28] for the Lennard-Jones function and from [15] for the inverse power relation.

The final component $\vec{R}_i$ of the particle-particle force is the reference force, which depends on the shape S of the ionic charge. As previously stated, the particle-particle portion of the force is calculated for ions within the relatively small spherical region Ω_i. The role of the reference force is to correct for the overlap between Ω_i and the entire system over which the mesh force $\vec{F}_i^{pm}$ is calculated. In other words, the sources of electrostatic force acting on a given charged particle are classified as "far sources" (including boundary conditions) that are accounted for efficiently by the Poisson solver, and "close sources" generating forces that are not resolved by the Poisson solver and must be computed by the expensive $O(N^2)$ particle-particle scheme. The domain Ω_i defines the fine resolution region around a given ion. For obvious reasons, the solution of Poisson's equation can not be obtained by subtracting the charges within Ω_i—this would indeed require a full solution for each particle at each iteration—so *the effect* of those sources is subtracted from the potential distribution *after* the solution has been obtained. This correction is accomplished by the reference force.

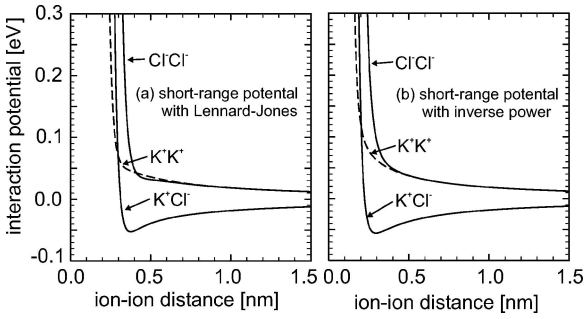

Figure 3. Comparison of short range Lennard-Jones and inverse power potential schemes for K+ and Cl− in an aqueous solution.

Clearly, the size of the Ω_i region should be chosen as small as possible based on performance considerations. The key aspect that limits the minimum size of Ω_i is the size of the ionic charge used for the charge assignment scheme (see Section 3.1). As stated above, the charge distribution is computed by assigning a "cloud" of charge to each individual ion. The cloud has a specific geometric shape and a predefined charge density. When calculating the total force on a given ion i, all the charged particles $j \neq i$ whose charge cloud is overlapping with the one of i must be considered "close sources" of the electrostatic force, and must be included in the domain Ω_i.

As stated in Section 3.1, the ionic electrostatic shape S chosen for this work is a sphere with an uniformly decreasing charge density, corresponding to the TSC weighting scheme [15]:

$$S(r) = \begin{cases} \dfrac{3}{\pi r_c}(r_c - r) & r_c \leq r \\ 0 & \text{otherwise} \end{cases}, \quad (24)$$

where r_c is the radius of the spherical charge "cloud". Therefore, the natural choice for the minimum cutoff radius that defines the short-range region Ω_i is twice r_c.

The reference force is then found analytically by substituting the shape function $S(r)$ into

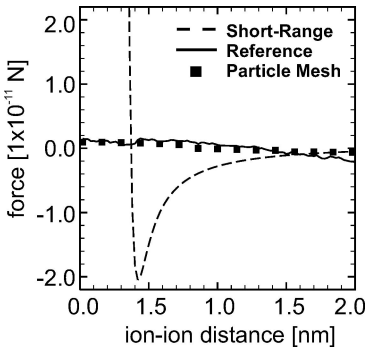

Figure 4. Components of the force between two ions of opposite charge in a 500 mM solution of KCl with no external bias.

Eq. (22):

$$R(r) = \frac{q_i q_j}{4\pi\epsilon_r\epsilon_0} \times \begin{cases} \frac{4}{35r_c^2}(224\zeta - 224\zeta^3 + 70\zeta^4 + 48\zeta^5 - 21\zeta^6) & 0 \le \zeta \le 1 \\ \frac{4}{35r_c^2}(12/\zeta^2 - 224 + 896\zeta - 840\zeta^2 + 224\zeta^3 & \\ \quad + 70\zeta^4 - 48\zeta^5 - 7\zeta^6) & 1 \le \zeta \le 2 \\ \frac{1}{r^2} & \text{otherwise} \end{cases} \tag{25}$$

where $\zeta = r/r_c$. To reduce the computational burden, the reference force is precomputed and tabulated as a function of the distance between ion pairs as suggested by Hockney [15] and, successively, by Wordelman [31].

The components of the force between an anion and a cation inside the short-range domain ($2r_c$=2 nm) are shown in Fig. 4 as a function of the inter-ionic separation. The two ions are placed in a 500 mM KCl solution, with no external bias. As expected, the reference force and mesh force have the same amplitude, and therefore will cancel within the short-range domain.

3.3. Time Discretization Scheme

The issue of time discretization is particularly relevant for the performance of the simulation code. As discussed in Section 2.1, the duration of the time-step must be carefully chosen to ensure self-consistency while minimizing the use of computational resources.

It should be noticed that, even if self-consistency requires a periodic update of the force fields, different components of the force evolve on different time scales, therefore allowing for different time-steps for the calculation of the mesh force, $\vec{F}_i^{pm}$, and the short-range particle-particle force, $\vec{F}_i^{pp}$. Such differentiation is used to optimize the use of computational resources.

The time-step used for updating the PP force is dictated by the time integration scheme of the ionic dynamics, as discussed in Section 2.1. In this case, the use of the Verlet-like scheme allows for relatively longer time-steps (20 fs) as compared with the standard Euler integration (5 fs).

Concerning the PM part of the force field, one observes that the evolution of the charge density over the grid can be correctly modeled with a less frequent update of the potential distribution [47,50,65]. Therefore, the Poisson time-step can be longer than the update time of the short-range force. As an estimator of the minimum characteristic time required to resolve the fluctuations in the long-range force we use the inverse of the plasma frequency [15],

$$\omega = \sqrt{\frac{c|q|^2}{\epsilon_r\epsilon_0 m}}, \tag{26}$$

where c is the ionic charge concentration, m is the ion mass and $|q|$ is the magnitude of the ion charge. The plasma frequency represents the electrostatic response of the system to a perturbation in the charge density. Therefore, the Poisson solver cannot properly accommodate electrostatic changes in the system if the PM time-step is larger than the inverse of this quantity. For an aqueous solution of KCl at 100 mM the inverse of the plasma frequency is approximately 5 ps which is several orders of magnitude longer than the time-step required to update the PP force.

Although in this work we use Eq. (26) to estimate the maximum tolerable duration of the Poisson time-step, it should be noted that the over-damped systems studied here are not rigorously described by plasma theory [15,66], and that an energetically stable ionic population can be modeled with less stringent limits for the Poisson time-step.

4. Computational Domain

A small cubic test volume representing a portion of a larger aqueous electrolytic solution is simulated

to validate the simulation tool. Dirichlet boundary conditions are set on opposite planes of the 3D simulation volume, while Neumann conditions [15] are imposed on the other four boundaries. In this way, an external electrostatic potential can be applied across the computational domain, and is included in the solution of Poisson's equation.

Ions are allowed to traverse the Dirichlet contact cells, and are specularly reflected by the Neumann boundaries. Since periodic boundary conditions are not imposed, an injection mechanism must be devised at the Dirichlet boundaries to maintain a given ion concentration in the computational domain without perturbing its energetic stability. In this work, since the simulated volume is assumed to represent only a portion of a larger electrolytic bath, the Dirichlet boundaries are kept at a constant concentration to mimic the effect of two far "electrodes". At each Poisson timestep an appropriate ion flux is imposed at the "electrodes", where the velocity of the injected ions is calculated with a Maxwellian distribution in the directions parallel to the contact cells and a half-Maxwellian in the normal direction. Within this injection scheme the average velocity of the injected particles does not correspond to the macroscopic flux, and the particles velocities (and energies) must relax to the steady-state values. This process is generally fast, and steady-state behavior is obtained within 2-3 grid cells from the Dirichlet boundary. To avoid artifacts introduced by the injecting "electrodes", several cells neighboring the contacts are excluded in the calculations of the bulk properties. Such an injection mechanism ensures a constant ionic concentration over long simulation times.

5. Simulation Results

In order to validate the proposed force-field scheme, the thermodynamic properties of an electrolytic solution are calculated under equilibrium conditions as a function of concentration, and are compared to values obtained with analytic approximations and experimental results, where available.

Additional simulations are also performed by introducing a 2 nm dielectric slab in the center of the computational domain, to mimic the presence of a lipid membrane with an externally applied transmembrane potential.

An important point of merit is that all the simulation results presented in this document have been obtained without any external dissipative mechanisms that enforce energy stability. For this reason the analysis of the stability of the ionic population plays a crucial role in the algorithmic choice.

5.1. *Thermodynamic Properties*

As an initial test, the equilibrium thermodynamic properties of an ionic solution are determined. This involves the calculation of the radial distribution function (RDF) [11], which relates the probability of finding a pair of ions at a specific separation to the probability in a homogeneous distribution at the same density [39]. The RDF as a function of the inter-particle distance is

$$g(r) = \frac{1}{\rho N}\left\langle \sum_i \sum_{j\neq i} \delta(\vec{r} - \vec{r}_{ij}) \right\rangle, \tag{27}$$

where $\vec{r}_{ij}$ is the particle separation, ρ is the ion density, and N is the time-averaged number of ions. The RDF provides important structural information about the system, and can be used to calculate the ensemble average of any pair function, including the free energy, pressure, and chemical potential [39]. The knowledge of these three functions allows for the calculation of all other observable thermodynamic quantities, and the comparison with the experiment.

The RDF for KCl and NaCl electrolytic solutions are shown in Fig. 5 and are compared with the numerical solution of the Ornstein-Zernike equation [45] solved using the hypernetted chain approximation (HNC) as a closure relation [11,67]. As can be seen, the RDFs obtained with the simulation approach proposed in this work show excellent agreement with the HNC results over a variety of concentrations and ionic species. The results of the HNC solver have been validated through comparisons with previously reported HNC simulations [28]. Details of the HNC method used to calculate the RDF are given in App. A.

Further comparisons have also been made of the osmotic coefficient [11,45] as computed with the proposed method, with the HNC, and with experimental values. The osmotic coefficient for a multi-ion system is calculated with the expression [45]:

$$\psi = 1 - \frac{1}{6\rho k_B T} \sum_{i,j} \rho_i \rho_j \times \sum_{r_k}^{r_{\max}} \frac{\partial u_{ij}(r_k)}{\partial r} g_{ij}(r_k) 4\pi r_k^3 \Delta r_k, \tag{28}$$

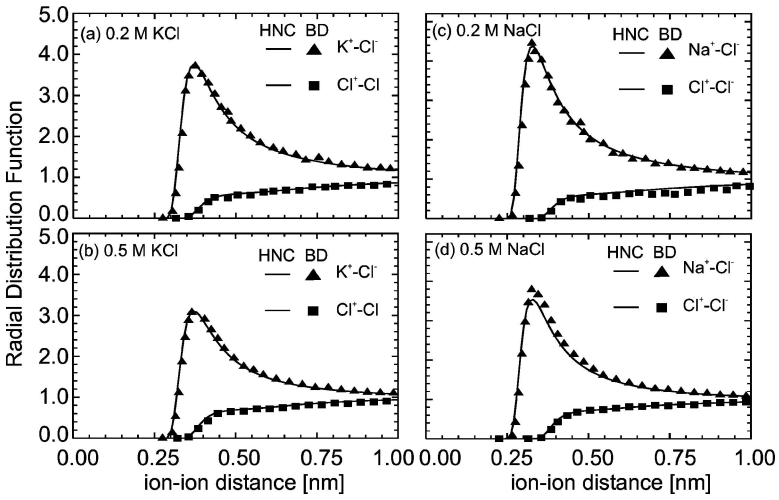

Figure 5. Radial distribution function as a function of distance for different concentrations of KCl and NaCl. Comparison with results from the HNC, shown as solid lines, show excellent agreement for different concentrations.

where ρ_i is the density of the ith species, u_{ij} is the particle-particle interaction potential, and $r_{\max}$ is the distance at which the contribution from spatial derivative of the potential u_{ij} is negligible. The RDF is written here as g_{ij} to distinguish between the different species i and j. A plot of the osmotic coefficient as a function of concentration is shown in Fig. 6 for KCl and NaCl, and includes the experimental values as well as the results of the HNC calculation. Although the agreement between the HNC and the Brownian dynamics is very good, there is a deviation from the experimental values, particularly for NaCl. Several factors can explain the discrepancy. First, the equilibrium pressure is a crucial component of the osmotic coefficient, and the ambient pressure of the computational representation differs with respect to the experimental system because of the implicit water model [45]. Also, the RDF is significantly dependent on the parameters used in the short-range interaction, and these vary considerably in literature, particularly for NaCl [68].

The computational domain used for these simulations is a cube with 20 nm sides and is discretized with a $20 \times 20 \times 20$ homogeneous tensor-product grid. The PM force is updated every 2 ps while the PP force is calculated every 20 fs. The integration scheme used for the simulations is the Verlet-like algorithm. The total simulated time is 2 ns and the system properties are determined by taking the ensemble average over the final 1.5 ns.

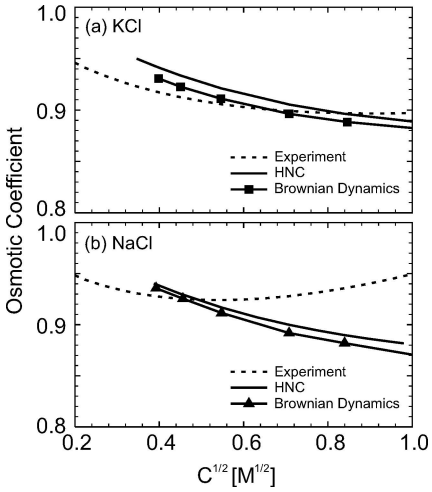

Figure 6. Osmotic coefficient versus concentration for (a) KCl and (b) NaCl. Results are compared with experimental values and with results from the HNC. The osmotic coefficient in this work is in very good agreement with the analytic model.

5.2. Transmembrane Potential

Another important validation of the force-field scheme comes from the calculation of the transmembrane potential. An impermeable dielectric slab representing a lipid membrane is embedded in the center of an electrolytic solution, and a simulation is run to determine the charge distribution at the water/lipid interface.

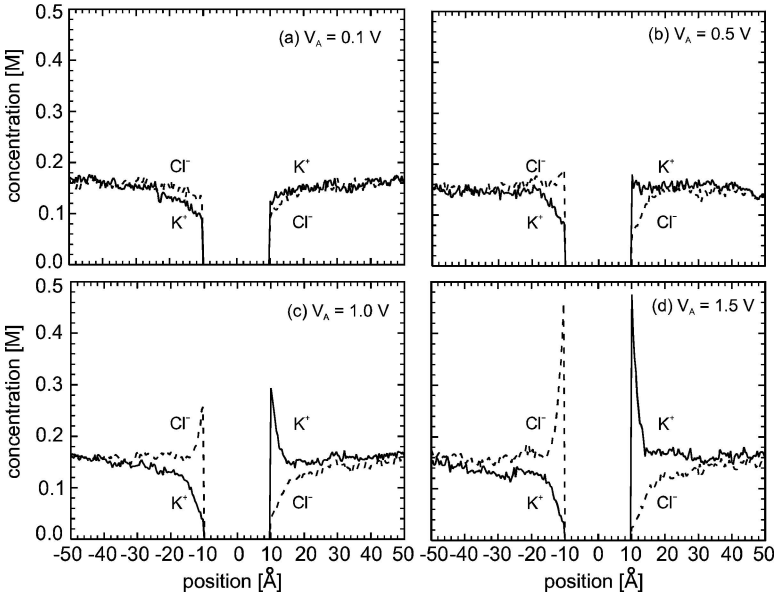

Figure 7. Average concentration of anions and cations in a 150 mM solution of KCl with a 2 nm dielectric membrane in the center.

The relative dielectric constant of the membrane and the surrounding bath is 2 and 80, respectively. External bias is applied at the electrodes. Due to the large difference in dielectric constants, most of the potential drop is across the membrane. The standard continuity condition of the electric displacement across the dielectric boundary [14] gives rise to an accumulation or depletion of ions at the edge of the membrane. The sign of the ionic charge and the external bias determines whether the ions are attracted to or repelled by the membrane surface. A plot of the average concentration of anions and cations for different bias voltages is shown in Fig. 7. The ion concentration is plotted along the direction normal to the membrane interface, and a spatial average is taken in the other two directions. The membrane is 2 nm wide and is contained in an electrolytic bath of 150 mM KCl. At low voltages, the distribution of ions is approximately homogeneous on both sides of the membrane (see Fig. 7(a)), but, with increasing bias, the K^+ ions accumulate on one side and deplete on the other, while the Cl^- ions assume the opposite configuration, as a consequence of Gauss' law. The concentration on the two sides of the domain is maintained during the simulation by the injection mechanism.

As opposed to other force field schemes, the proposed approach allows for simulations with asymmetric ionic concentrations. Figure 8 shows a plot of the average ionic distribution and the potential profile in a

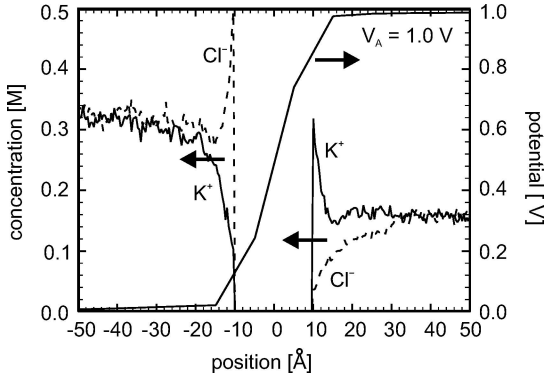

Figure 8. Average ionic concentration and potential distribution in a KCl bath separated by a 2 nm dielectric membrane. The concentration on the left side is 300 mM, while the one on the right is 150 mM.

system with 300 mM KCl on the left side of the membrane and 150 mM KCl on the right. According to the behavior of the Boltzmann distribution [11], the net accumulation or depletion of ionic charge is equal on the two sides of the membrane.

The transmembrane potential simulations are performed on the same geometric configuration used for the study of the thermodynamic properties, as described in Section 5.1. The Euler integration scheme is used, and the PP force is updated every 5 fs, while the Poisson time-step is 2 ps. Simulations are run for 5 ns with averages taken over the last 4 ns.

6. Conclusions

In this work, a force-field scheme based on a Poisson P^3M algorithm is proposed as an accurate and efficient tool to simulate ionic charge transport in electrically inhomogeneous systems. The force-field scheme is self-consistently coupled with a dynamics simulation kernel based on the Langevin equation. Calculations of thermodynamic properties of different electrolytic solutions are performed, and show excellent agreement with other models. In addition, the spatial charge distribution profile in the presence of a double dielectric interface is obtained. This work represents an initial step toward the development of an efficient and robust simulation tool for the particle-based modeling of complex inhomogeneous biological systems, such as lipid membranes and ion channels. The proposed approach will be applied to MD simulations to further validate it and investigate its advantages and limitations.

Appendix A: Hypernetted-Chain Method

The hypernetted-chain approximation (HNC) supplies a closure relation for the Ornstein-Zernicke (OZ) equation, which is a non-linear integral equation for the radial distribution function in terms of the intermolecular potential [45].

The OZ equation for a mixture of several species is given by [11],

$$h_{ss'}(r_{ij}) = c_{ss'}(r_{ij}) + \sum_l \rho_l \int h_{sl}(r_{ik}) c_{ls'}(r_{jk}) dr_3, \tag{29}$$

$$= g_{ss'}(r_{ij}) - 1, \tag{30}$$

where $c_{ss'}(r_{ij})$ and $g_{ss'}(r_{ij})$ are the direct correlation function and pair correlation function (radial distribution function), respectively between particle i of species s and particle j of species s'. The integral term in Eq. (29) is an indirect component of the correlation function, and represents the correlation of particle i with particle j initially propagated through a third particle (either directly or indirectly).

A closure relation for Eq. (29) is obtained by determining an expression for $c_{ss'}(r_{ij})$ in terms of $g_{ss'}(r_{ij})$, and substituting this new expression into Eq. (29). Within the HNC formulation, the direct correlation function is expressed as the difference between the total correlation function and the indirect correlation function, or,

$$c_{ss'}(r_{ij}) = g_{ss'}(r_{ij}) - g^{\text{ind}}_{ss'}(r_{ij}), \tag{31}$$

where $g^{ind}_{ss'}(r_{ij})$ is the radial distribution function corresponding to a system without the direct (*i.e.*, pairwise) interaction, also called the indirect radial distribution function:

$$g^{\text{indirect}}_{ss'}(r_{ij}) = e^{-[w_{ss'}(r_{ij}) - u_{ss'}(r_{ij})]/K_B T}, \tag{32}$$

where w is the total interaction potential (potential of mean force) and u is the pairwise particle-particle interaction. By Taylor-expanding the indirect radial distribution function,

$$g^{\text{indirect}}_{ss'}(r_{ij}) = \frac{1}{k_B T}[w_{ss'}(r_{ij}) - u_{ss'}(r_{ij})] - 1, \tag{33}$$

and substituting it into Eq. (31), one finally obtains the HNC equation:

$$c_{ss'}(r_{ij}) = g_{ss'}(r_{ij}) - 1 - n_{ss'}(r_{ij}), \tag{34}$$

where

$$n_{ss'}(r_{ij}) = \frac{1}{k_B T}[w_{ss'}(r_{ij}) - u_{ss'}(r_{ij})]. \tag{35}$$

The radial distribution function is then calculated iteratively from the following set of coupled matrix equations [69]:

$$\mathbf{c}(\mathbf{r}) = \mathbf{g}(\mathbf{r}) - \mathbf{1} - \mathbf{n}(\mathbf{r}) \tag{36}$$

$$\hat{\mathbf{n}}(\mathbf{q}) = \hat{\mathbf{c}}(\mathbf{q})/(\mathbf{1} - \rho\hat{\mathbf{c}}(\mathbf{q})) - \hat{\mathbf{c}}(\mathbf{q}) \tag{37}$$

$$\mathbf{g}(\mathbf{r}) = \exp[(\mathbf{n}(\mathbf{r}) - \mathbf{u}(\mathbf{r}))/k_B T], \tag{38}$$

where $\hat{\mathbf{c}}(\mathbf{q})$ denotes the three dimensional Fourier transform. The bold face notation is used to represent matrix quantities. This set of equations is discretized on a real-space grid with 0.1 Å uniform spacing. The maximum particle separation is set to 2 nm. The solution is obtained when the following convergence criterion is satisfied [69]:

$$\epsilon_{th} \geq \left[\int_0^\infty \left|c^k(r) - c^{k+1}(r)\right|^2 dr\right]^{1/2}, \tag{39}$$

where ϵ_{th} is the convergence threshold and k represents the iteration step. According to published values [69], the convergence threshold in this work is set to 10^{-14}.

Following the work of Ng [69] and Belloni [70], the function

$$u^{l}_{ss'}(r_{ij}) = \frac{2q_s q'_s}{8\pi\epsilon_0\epsilon_r r_{ij}}\,\mathrm{erfc}(\alpha r_{ij}), \qquad (40)$$

where α determines the spatial distance of the coulombic potential, is subtracted from the pairwise interaction to eliminate the divergence in the Fourier transform of the potential.

Acknowledgments

This work was partially supported by the National Institute of Health training grant T32 HL07692

References

1. B. Hille, *Ionic Channels of Excitables Membranes* (Sinauer, Massachusetts, 3rd edition, 2001).
2. E. Neher and B. Sakmann, "Single-Channel currents recorded from membrane of denervated frog muscle fibers," *Nature*, **260**, 799 (1976).
3. F.M. Ashcroft, *Ion channels and Disease* (Academic Press, S. Diego, CA, 2000).
4. M. Goryll, S. Wilk, G.M. Laws, T. Thornton, S. Goodnick, M. Saraniti, J. Tang, and R.S. Eisenberg, "Silicon-based ion channel sensor," *Superlattices and Microstructures* 2004 (in press).
5. S.M. Sze, *Physics of Semiconductor Devices* (2nd edition, John Wiley & Sons, New York, 1981).
6. Semiconductor Industry Association, *International Technology Roadmap for Semiconductors*, chapter "Process integration, devices, and structures," (International SEMATECH, Austin - TX, 1999) p. 83.
7. G. Lamm, *The Poisson-Boltzmann Equation*, vol. 19 of *Reviews in Computational Chemistry* (VHC Publishers, 2003) chap. 4, p. 147.
8. R.S. Eisenberg, M.M. Klosek, and Z. Schuss, "Diffusion as a chemical reaction: Stochastic trajectories between fixed concentrations," *Journal of Chemical Physics*, **102**(4), 1767 (1995).
9. S.-H. Chung, T.W. Allen, and S. Kuyucak, "Modeling diverse range of potassium channels with Brownian dynamics," *Biophysical Journal*, **83**(1), 263 (2002).
10. W. Im and B. Roux, "Ions and counterions in a biological channel: A molecular dynamics simulation of OmpF porin from escherichia coli in an explicit membrane with 1 M KCl aqueous salt solution," *Journal of Molecular Biology*, **319**(5), 1177 (2002).
11. D.A. McQuarrie, *Statistical Mechanics* (University Science Books, Sausalito, CA, 2000).
12. C.L. Brooks, B.M. Pettitt, and M. Karplus, "Structural and energetic effects of truncating long ranged interactions in ionic and polar fluids," *Journal of Chemical Physics*, **83**(11), 5897 (1985).
13. L. Perera, U. Essmann, and M.L. Berkowitz, "Effect of the treatment of long-range forces on the dynamics of ions in aqueous solutions," *Journal of Chemical Physics*, **102**(1) (1995).
14. J.D. Jackson, *Classical Electrodynamics* (2nd edition John Wiley & Sons, New York 1975).
15. R.W. Hockney and J.W. Eastwood, *Computer Simulation Using Particles*. (Adam Hilger, Bristol, 1988).
16. W. Hackbush, *Multi-Grid Methods and Applications* (Springer –Verlag, Berlin, 1985).
17. N.W. Ashcroft and N.D. Mermin, *Solid State Physics* (Holt–Sauders International Editions, Tokyo, 1981).
18. M.V. Fischetti and S.E. Laux, "Monte Carlo analysis of electron transport in small semiconductor devices including band-structure and space-charge effects," *Physical Review B*, **38**(14), 9721 (1988).
19. W.J. Gross, D. Vasileska, and D.K. Ferry, "Ultrasmall MOSFETs: the importance of the full Coulomb interaction on device characteristics," *IEEE Transactions on Electron Devices*, **47**(10), 1891 (2000).
20. C.J. Wordelman and U. Ravaioli, "Integration of a particle-particle-particle-mesh algorithm with the ensamble Monte Carlo method for the simulation of ultra- small semiconductor devices," *IEEE Transaction on Electron Devices*, **47**(2), 410 (2000).
21. A.R. Leach, *Molecular Modeling. Principles and Applications*, 2nd edition (Prentice Hall, Harlow, England, 2001).
22. P. Gibbon and G. Sutmann, "Long-range interactions in many-particle simulation," in *Quantum Simulations of Many-Body Systems: From Theory to Algorithms, Lecture Notes*, edited by J. Grotendorst, D. Marx, and A. Muramatsu, vol. 10 of *NIC*, John von Neumann Institute for Computing, Jülich, Germany, 2002) p. 467.
23. P. Ewald, "Die Berechnung optischer und elektrostatischer Gitterpotentiale," *Annalen der Physik*, **64**, 253 (1921).
24. D.R. Rapaport, *The Art of Molecular Dynamics Simulation* (Cambridge University Press, Cambridge, UK, 1995).
25. A. Brandt, "Multi-level adaptive solutions to boundary-value problems, *Mathematics of Computation*, **31**(138), 333 (1977).
26. M. Hoyles, S. Kuyucak, and S.-H. Chung, "Solutions of Poisson's equation in channel-like geometries," *Computer Physics Communications*, **115**(1), 45 (1998).
27. S.C. Li, M. Hoyles, S. Kuyucak, and S.-H. Chung, "Brownian dynamics study of ion transport in the vestibule of membrane channels," *Biophysical Journal*, **74**(1), 37 (1998).
28. W. Im, S. Seefeld, and B. Roux, "A grand canonical Monte Carlo-Brownian dynamics algorithm for simulating ion channels," *Biophysical Journal*, **79**(2), 788 (2000).
29. D.L. Ermak, "A computer simulation of charged particles in solution. I, "Technique and equilibrium properties," *Journal of Chemical Physics*, **62**(10), 4189 (1975).
30. P. Turq, F. Lantelme, and H.L. Friedman, "Brownian dynamics: Its application to ionic solutions," *Journal of Chemical Physics*, **66**(7), 3039 (1977).
31. M.A. Wilson, A. Pohrille, and L.R. Pratt, "Molecular dynamic test of the Brownian description of Na^+ motion in water," *Journal of Chemical Physics*, **83**(11), 5832 (1985).

32. K. Cooper, E. Jakobsson, and P. Wolynes., "The theory of ion transport through membrane channels," *Progress in Biophysis and Molecular Biology*, **46**(1), 51 (1985).
33. E. Jakobsson and S.-W. Chiu, "Stochastic theory of ion movement in channels with single-ion occupancy. Application to sodium permeation of gramicidin channels," *Biophysical Journal*, **52**(1), 33 (1987).
34. S. Bek and E. Jakobsson, "Brownian dynamics study of a multiply-occupied cation channel: application to understanding permeation in potassium channels, *Biophysical Journal*, 66(4), 1028, 1994.
35. S.-H. Chung, T.W. Allen, M. Hoyles, and S. Kuyucak, "Permeation of ions across the potassium channel: Brownian dynamics studies," *Biophysical Journal*, **77**(5), 2517 (1999).
36. S.-H. Chung, T.W. Allen, and S. Kuyucak, "Conducting-state properties of the KcsA potassium channel from molecular and Brownian dynamics simulations," *Biophysical Journal*, **82**(2), 628 (2002).
37. B. Corry, M. Hoyles, T.W. Allen, M. Walker, S. Kuyucak, and S.-H. Chung, "Reservoir boundaries in Brownian dynamics simulations of ion channels," *Biophysical Journal*, **82**(4), 1975 (2002).
38. C.R. Arokianathan, A. Asenov, and J.H. Davies, "An approach based on Brownian motion for the simulation of ultrasmall semiconductor devices," *Journal of Applied Physics*, **81**(1), 226 (1996).
39. M.P. Allen and D.J. Tildesley, *Computer Simulation of Liquids* (Clarendon Press, Oxford, 1987).
40. F.O. Raineri, M.D. Wood, and H.L. Friedman, "Self-diffusion coefficients of ions in electrolyte solutions by nonequilibrium Brownian dynamics," *Journal of Chemical Physics*, **92**(1), 649 (1990).
41. M. Canales and G. Sesé, "Generalized Langevin dynamics simulations of NaCl electrolyte solutions," *Journal of Chemical Physics*, **109**(14), 6004 (1998).
42. M. Jarat, O. Bernard, P. Turq, and G.R. Kneller, "Transport coefficients of electrolyte solutions from Smart Brownian Dynamics simulations," *Journal of Chemical Physics*, **110**(16), 7993 (1999).
43. S. Yang, H. Han, and S. Lee, "An efficient Brownian dynamics method for evaluating inertial dynamics effects on diffusion–influenced reactions," *Journal of Physical Chemistry B*, **105** (25), 6017 (2001).
44. J.F. Dufreche, M. Jardat, T. Olynyk, O. Bernard, and P. Turq, "Mutual diffusion coefficient of charged particles in the solvent fixed frame of reference from Brownian dynamics simulation," *Journal of Chemical Physics*, **117**(8), 3804 (2002).
45. J.M.G. Barthel, H. Krienke, and W. Kunz, *Physical Chemistry of Electrolyte Solutions*, Number 5 in Topics in Physical Chemistry (Springer, New York, 1998).
46. W.F. van Gunsteren and H.J.C. Berendsen, "Algorithms for Brownian dynamics," *Molecular Physics*, **45**(3), 637 (1982).
47. E. Barth and T. Schlick, "Extrapolation versus impulse in multiple-timestepping schemes. II. Linear analysis and applications to Newtonian and Langevin dynamics," *Journal of Chemical Physics*, **109**(5), 1633 (1998).
48. S.K. Gray, D.W. Noid, and B.G. Sumpter, "Sympletctic integrators for large scale molecular dynamics simulations: A comparison of several explicit methods," *Journal of Chemical Physics*, **101**(5), 4062 (1994).
49. L. Verlet, "Computer 'experiments' on classical fluids. I. Thermodynamical properties of Lennard-Jones molecules," *Physical Review*, **159**(1), 159 (1967).
50. T. Schlick, *Molecular Modeling and Simulation: An Interdisciplinary Guide*, vol. 21 of *Interdisciplinary Applied Mathematics* (Springer, New York, 2000).
51. R.S. Varga, "Factorization and normalized iterative methods," in *Boundary Problems in Differential Equations*, edited by R. E. Langer (University of Wisconsin Press, Madison, Wisconsin, 1960) p. 121.
52. D.M. Young, *Iterative Solution of Large Linear Systems* (Computer Science and Applied Mathematics. Academic Press, New York, 1971).
53. R.S. Varga, *Matrix Iterative Analysis*. Series in Automatic Computation (Prentice–Hall, Englewood Cliffs, N.J., 1962).
54. S. Selberherr, *Analysis and Simulation of Semiconductor Devices* (Springer–Verlag, Vienna, New York, 1984).
55. S. Aboud, D. Marreiro, M. Saraniti, and R. Eisenberg. A poisson P^3M force field scheme for particle-based simulations of ionic liquids: Complementary material. ftp://ftp.rush.edu/pub/Eisenberg/Saraniti/JCEL04.pdf (August 2005).
56. M. Saraniti, A. Rein, G. Zandler, P. Vogl, and P. Lugli, "An efficient multigrid poisson solver for device simulations," *IEEE Transaction on Computer–aided Design of Integrated Circuits and Systems*, **15**(2), 141 (1996).
57. G. Dahlquist and Å. Björck, *Numerical Methods* (Prentice–Hall, Englewood Cliffs, N.J., 1974).
58. A. Brandt, "Multigrid solvers on parallel computers," in *Elliptic Problem Solvers*, edited by M. H. Schultz (Academic Press, New York, 1981) p. 39.
59. J.V.L. Beckers, C.P. Lowe, and S.W. De LeeuW, "An itrative PPPM method for simulating coulombic systems on distributed memory parallel computers," *Molecular Simulation*, **20**, 369 (1998).
60. H.L. Stone, "Iterative solution of implicit approximations of multidimensional partial differential equations," *SIAM Journal of Numerical Analysis*, **5**(3), 530 (1968).
61. J.A. Meijerink and H.A. van der Vorst, "An iterative solution method for linear systems of which the coefficient matrix is a symmetric S-matrix," *Mathematics of Computation*, **31**, 148 (1977).
62. J. Ayubi-Moak, S. Wigger, S. Goodnick, and M. Saraniti, 3D biconjugate gradient-multi grid coupling schemes for field equations in semiconductor device simulation, in *Proceedings of 2002 International Conference on Modeling and Simulation of Microsystems - MSM2002*, April 2002. Accepted for poster presentation.
63. P.S. Ramanathan and H.L. Friedman, "Study of a refined model for aqueous 1-1 electrolytes," *Journal of Chemical Physics*, **54**(3), 1086 (1971).
64. R.S. Berry, S.A. Rice, and J. Ross, *Physical Chemistry*, 2 edition. (Oxford University Press, May 2000).
65. M. Tuckerman, B.J. Berne, and G.J. Martyna, "Molecular dynamics algorithm for multiple time scales: Systems with long range forces," *Journal of Chemical Physics*, **94**(10), 6811 (1991).

66. C.K. Birdsall and A.B. Langdon, *Plasma Physics via Computer Simulation* (Institute of Physics Publishing, Bristol and Philadelphia, 1991).
67. J.P. Hansen and I.R. McDonald, *Theory of Simple Liquids* (Academic, London, 1976).
68. M. Patra and M. Karttunen, "Systematic comparison of force fields for microscopic simulations of NaCl in aqueous solutions: Diffusion and structural properties," *Journal of Computational Chemistry*, **25**, 678 (2004).
69. K.-C. Ng, "Hypernetted chain solutions for the classical one-componenet plasma up to $\gamma = 7000$," *Journal of Chemical Physics*, **61**, 2680 (1974).
70. L. Belloni, "A hypernetted chain study of highly asymmetrical polyelectrolytes," *Chemical Physics*, **99**, 43 (1985).